scientific reports

Check for updates

OPEN

Mathematical models of apparent viscosity as a function of water–cement/binder ratio and superplasticizer in cement pastes

Yong Yuan[1], Xiaoyun Wang[1], Xi Chen[2], Peng Xiao[3], Eduardus Koenders[3] & Ying Dai[4]✉

The water–cement/binder ratio and the admixture of water-reducing agents strongly affect the rheological properties of cement pastes. This study develops mathematical models to predict the apparent viscosity of cement pastes with varying water-cement/binder ratios and polycarboxylate-based superplasticizer content by introducing the power law shear stress-shear strain relation of non-Newtonian fluids into the Navier–Stokes motion equations. The developed models are compared with the results of rheological experiments and verified for their accuracy in simulating the apparent viscosity of cement pastes. These models provide insight into the rheological behaviour of cement pastes and could have practical applications in the construction industry.

Abbreviations

$\frac{D}{Dt}$	Material derivative
ρ	Density of fluid
P	Liquid pressure
η	Apparent viscosity
u_i	Liquid velocity in i ($i = 1, 2, 3$) direction
f_i	Body force on unit volume
t	Time variable
P_0	Initial water pressure
ϕ	Volume fraction of solid
ϕ^c	Volume fraction of water
w/b	Water–binder ratio
w/c	Water–cement ratio
u_s	Velocity of solid
m_s	Mass of solid
ρ_s	Density of solid
∇	Laplace operator
τ	Shear stress
$\dot{\gamma}$	Shear rate
K	Coefficient of Ostwald model
n	Index of Ostwald model
k	Coulomb's constant
q_1,q_2	Charges of ions
r	Distance of two ions
F_{et}	Electrostatic repulsion force

[1]College of Civil Engineering, Tongji University, Shanghai 200092, China. [2]College of Civil Engineering and Architecture, Jiaxing University, Zhejiang 314001, China. [3]Institute of Construction and Building Materials, Technical University of Darmstadt, 64287 Darmstadt, Germany. [4]School of Aerospace Engineering and Applied Mechanics, Tongji University, Zhangwu Road 100, Shanghai 200092, China. ✉email: ydai@tongji.edu.cn

n_S Dosage of superplasticizer
F_s Steric hindrance force

The rheology of fresh cement paste is closely linked to its workability, primarily determined by the water-cement ratio *(w/c)*[1–4]. After adding mineral admixtures to cementitious materials, the water-binder ratio *(w/b)* is used instead[5]. Numerous rheological models have been developed to characterize the rheological properties of cement pastes. For example, Einstein[6] proposed a rigid sphere suspension model with a linear relationship between viscosity and solid volume fraction, closely related to *w/c* or *w/b*[7]. Other models with non-linear relationships, such as the power law (Krieger-Dougherty model), exponential law (Mooney model), and fraction forms (Eilers model, Robinson model, Quemada model, et al.)[8–10], have been applied to describe non-linear results in cement pastes.

Several rheological models have been used to analyse the evolution of shear stress with shear rate and *w/c* in cement pastes or similar materials[4,11–17]. These models include the Bingham model which presents a linear relationship between shear stress and shear rate[11,13], and the modified Bingham model which applies quadratic functions to discuss the non-linear parts of the shear stress-shear rate in fresh pastes[12]. Other models, such as the Casson model which adds a square root function of the shear rate to the Bingham model[13], and the Ostwald model which uses a power law to obtain the whole constitutive relation between shear stress and shear rate[14], have also been employed. The Herschel–Bulkey model combines the Bingham model and the Ostwald model[15,16], while the Bingham–Papanastasiou model has a Papanastasiou's function multiplier based on the Bingham model[4]. The Vipulanandan model takes a fraction function as the shear rate[17]. The parameters in these models are often adjusted based on experimental results from rheological tests with various shear protocols[14], and they often change as *w/c* varies[4].

Apparent viscosity, an important rheological index, is influenced by several factors, including hydration degree, thixotropy, and the dosage of additives and admixtures[14]. The experimental rheological results of Liu et al.[18], shown in Fig. 1, demonstrate the relations between the apparent viscosity and the shear rate of cement pastes. These relations change with the *w/b* and the dosage of superplasticizer (SP). The cement pastes can show shear thickening behavior[18], for cement paste with lower *w/b* and a high dosage of SP, as shown in Fig. 1b and c.

Most of the present models are developed based on the test results in rheological experiments to consider the influence of *w/c*, additives, and admixtures. The representatives of the models are Jones and Taylor's model (six-parameter exponential form)[19], Lapasin et al. model (linear function of *w/c*)[20], Ivanov and Roshavelov

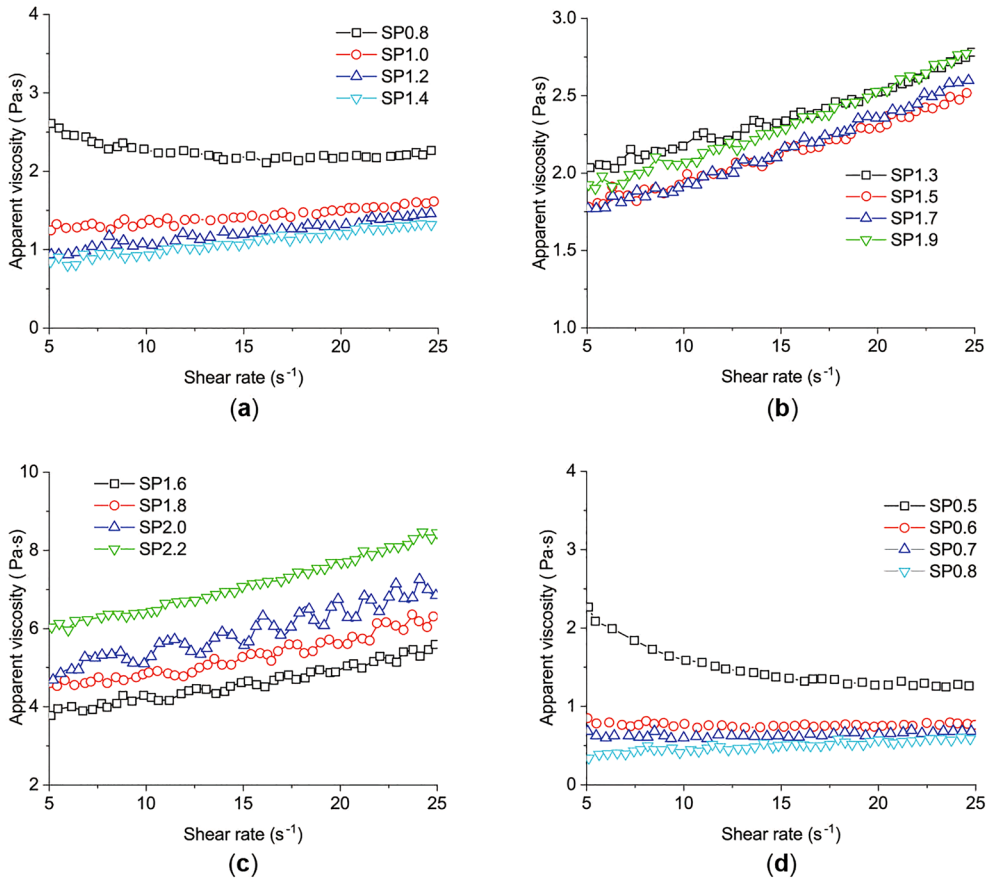

Figure 1. The relations between the apparent viscosity and the shear rate for pastes with different *w/b*[18]. (**a**) paste with w/b = 0.24, (**b**) paste with w/b = 0.20, (**c**) paste with w/b = 0.16, (**d**) paste with w/b = 0.32.

model (twenty-parameter polynomial with *w/c*, SP, silica fume, tricalcium aluminate and sulfur trioxide)[21], and Rosquoët model (linear function of *w/c* and power law of the shear rate)[22]. Other empirical formulations consider the yield stress in the Bingham model[14], the Herschel–Bulkey model[14], the YODEL model[23,24], and the Ma & Kawashima model[25] as a fractional or exponential function of the cement volume fraction.

Different from the experimental or empirical method, the target of this paper is to give a theoretical explanation of the change in the viscosity of cement pastes considering *w/c(w/b)* and SP based on mathematical derivations. Firstly, the Ostwald model is introduced into the Navier–Stokes equations of solid mixing with liquid. Next, an ordinary differential equation is derived by the mean value theorem in a tiny domain. To solve the ordinary differential equation, the Bernstein polynomial approximation is applied in the whole domain to derive a concise mathematical model. The model is a four-parameter formulation of the shear stress-shear rate for cement pastes with one variable *w/c*. More importantly, by introducing the electrostatic repulsion and steric hindrance into the Navier–Stokes equations, the influence of the SP can be quantitively considered by a function of its dosage. Correspondingly, the mathematical model can be extended to present the shear stress changes with the shear rate, *w/c*, and SP, with the same four-parameter formulation. The developed model is verified by being compared with the experimental results from Rosquoët et al.[22], Jeong et al.[4], Cyr et al.[26], and Liu et al.[18].

Method

The apparent viscosity model with *w/c*

According to Kundu et al.[27], the Navier–Stokes equations are

$$\frac{D(\rho u_i)}{Dt} = -\frac{\partial P}{\partial x_i} + \nabla(\eta \nabla u_i) + \rho f_i \tag{1}$$

in which $\frac{D}{Dt}$ is the material derivative, ρ is the density of the fluid, P is the liquid pressure, η is the apparent viscosity of the fluid, u_i is the velocity in the x_i ($i = 1, 2, 3$) direction, f_i is the body force on a unit volume of the fluid. In the Cartesian coordinate system, $O\text{-}x_1x_2x_3$, i ($i = 1, 2, 3$) corresponds to the x, y, and z axis respectively.

A simply unidirectional flow with constant pressure is considered, therefore the Newton's law of viscosity is applicable as

$$\begin{cases} u_1 = u(y,t) \\ u_2 = 0 \\ u_3 = 0 \\ P = P_0 \end{cases} \tag{2}$$

where u_1 depends on the space variable y and the time variable t, P_0 is the initial pressure. By substituting Eq. (2) into Eq. (1), Eq. (3) is obtained

$$\frac{\partial(\rho u)}{\partial t} = \frac{\partial}{\partial y}\left(\eta \frac{\partial u}{\partial y}\right) + \rho f_x. \tag{3}$$

Considering the procedure of mixing the solid and the liquid to produce fresh cement paste[28], Eq. (3) is changed into

$$\frac{\partial(\phi^c \rho u)}{\partial t} = \phi^c \frac{\partial}{\partial y}\left(\eta \frac{\partial u}{\partial y}\right) + \phi^c \rho f_x \tag{4}$$

in which ϕ^c, the volume fraction of liquid, can be taken as water in cement paste

$$\phi^c = 1 - \phi \tag{5}$$

here ϕ, the volume fraction of solid, can be taken as the binder particles for cement with additives such as silica fume and fly ash. The solid phase serves as the structural phase in the paste and is assumed to sustain the body force of the liquid phase. By introducing the drag force, we have

$$\frac{d}{dt}(\phi m_s u_s) = -\phi^c \rho f_x \tag{6}$$

where u_s and m_s are the velocity and the mass of the solid respectively. In unit volume, m_s can be expressed as

$$m_s = \phi \rho_s \tag{7}$$

ρ_s is the density of the solid. Substituting Eqs. (5)–(7) into Eq. (4), it is obtained

$$\frac{\partial[(1-\phi)\rho u + \phi \rho_s u_s]}{\partial t} = (1-\phi)\frac{\partial}{\partial y}\left(\eta \frac{\partial u}{\partial y}\right). \tag{8}$$

In a tiny time increment Δt, the variables ϕ and ρ_s own little changes. Ignoring the variation of ϕ and ρ_s, Eq. (8) can be written as

$$\frac{1}{\phi \rho_s} \frac{\partial\left[\phi \rho_s \left(\frac{(1-\phi)\rho}{\phi \rho_s} u + u_s\right)\right]}{\partial t} = \frac{(1-\phi)}{\phi \rho_s} \frac{\partial}{\partial y}\left(\eta \frac{\partial u}{\partial y}\right) \tag{9}$$

where w/b is given as

$$w/b = \frac{(1-\phi)\rho}{\phi\rho_s}. \tag{10}$$

Then, Eq. (9) is changed into

$$\frac{1}{\phi\rho_s}\frac{\partial[\phi\rho_s((w/b)u+u_s)]}{\partial t} = \frac{w/b}{\rho}\frac{\partial}{\partial y}\left(\eta\frac{\partial u}{\partial y}\right). \tag{11}$$

The shear rate $\dot{\gamma}$ is

$$\dot{\gamma} = \frac{\partial u}{\partial y}. \tag{12}$$

Substituting it into Eq. (11), we have

$$\frac{1}{\phi\rho_s}\frac{\partial[\phi\rho_s((w/b)u+u_s)]}{\partial t} = \frac{w/b}{\rho}\frac{\partial}{\partial y}(\eta\dot{\gamma}). \tag{13}$$

In pure cement pastes, the value of w/b is

$$w/b = w/c \tag{14}$$

According to Ostwald[14], the power law shear stress-shear rate relation is

$$\tau = K\dot{\gamma}^n \tag{15}$$

where K and n are the calculation parameters. Then the apparent viscosity can be expressed as

$$\eta = \frac{\tau}{\dot{\gamma}} = K\dot{\gamma}^{n-1}. \tag{16}$$

In fact, the apparent viscosity in Eq. (16) can be affected by many factors, e.g., w/c, cement components, mixing time, standing time before measurement, and the degree of hydration[17,18]. When the cement components, the mixing time, the standing time before measurement, and the degree of hydration are determined, the viscosity is a function of the w/c

$$\eta = \eta(\mathrm{w/c}) \tag{17}$$

which means the parameters K and n might be the function of w/c as

$$\begin{cases} K = K(\mathrm{w/c}) \\ n = n(\mathrm{w/c}) \end{cases}. \tag{18}$$

Substituting Eq. (16) into Eq. (13), we have

$$\frac{1}{\phi\rho_s}\frac{\partial[\phi\rho_s((w/c)u+u_s)]}{\partial t} = \frac{w/c}{\rho}\frac{\partial}{\partial y}\left(K\dot{\gamma}^n\right). \tag{19}$$

In a tiny space increment Δy, it can be approximated as

$$K \approx \left(\frac{\partial\dot{\gamma}^n}{\partial y}\right)^{-1}\frac{\rho}{\phi\rho_s}\frac{\partial\left[\phi\rho_s\left(u+\frac{u_s}{(w/c)}\right)\right]}{\partial t}. \tag{20}$$

According to Eq. (10), the solid volume fraction ϕ is

$$\phi = \frac{\rho}{(w/c)\rho_s+\rho}. \tag{21}$$

Substituting Eq. (21) into Eq. (20), it is obtained

$$K \approx \left(\frac{\partial\dot{\gamma}^n}{\partial y}\right)^{-1}\frac{(w/c)\rho_s+\rho}{\rho_s}\frac{\partial\left[\frac{\rho\rho_s}{(w/c)\rho_s+\rho}\left(u+\frac{u_s}{(w/c)}\right)\right]}{\partial t}. \tag{22}$$

In the Δy, $\frac{\partial\dot{\gamma}^n}{\partial y}$ is approximately considered as a constant. It means K can be determined by w/c in a tiny domain $(w_0/c_0, w/c)$, where w_0/c_0 is an arbitrary known water cement ratio in the concrete mix proportion of interest and w/c is close to w_0/c_0. Then, K can be given by the Lagrange mean value theorem in the tiny domain

$$K = K|_{w/c=w_0/c_0} + K_1[(w/c)-(w_0/c_0)] \tag{23}$$

in which

$$K_1 = \frac{\partial K}{\partial (w/c)}|_{w/c=\Delta w} \tag{24}$$

and

$$\Delta w = w_0/c_0 + \theta[(w/c) - (w_0/c_0)] \tag{25}$$

where $\theta \in (0, 1)$. Substituting Eq. (23) into Eq. (22), it is derived

$$K|_{w/c=w_0/c_0} + K_1[(w/c) - (w_0/c_0)] = \left(\frac{\partial \dot{\gamma}^n}{\partial y}\right)^{-1} \frac{(w/c)\rho_s + \rho}{\rho_s} \frac{\partial \left[\frac{\rho\rho_s}{(w/c)\rho_s + \rho}\left(u + \frac{u_s}{(w/c)}\right)\right]}{\partial t}. \tag{26}$$

In the increment Δt, w/c owns little changes, the right side of Eq. (26) can be approximated as.

$$\left(\frac{\partial \dot{\gamma}^n}{\partial y}\right)^{-1} \frac{(w/c)\rho_s + \rho}{\rho_s} \frac{\partial \left[\frac{\rho\rho_s}{(w/c)\rho_s + \rho}\left(u + \frac{u_s}{(w/c)}\right)\right]}{\partial t} \approx \left(\frac{\partial \dot{\gamma}^n}{\partial y}\right)^{-1} \frac{\rho}{\rho_s} \frac{\partial u}{\partial t} + \left(\frac{\partial \dot{\gamma}^n}{\partial y}\right)^{-1} \frac{\rho}{(w/c)\rho_s} \frac{\partial u_s}{\partial t}. \tag{27}$$

Then Eq. (26) can be changed as

$$(w/c)K|_{w/c=w_0/c_0} + (w/c)aK_1 \approx (w/c)\left(\frac{\partial \dot{\gamma}^n}{\partial y}\right)^{-1} \frac{\rho}{\rho_s} \frac{\partial u}{\partial t} + \left(\frac{\partial \dot{\gamma}^n}{\partial y}\right)^{-1} \frac{\rho}{\rho_s} \frac{\partial u_s}{\partial t} \tag{28}$$

where

$$a = (w/c) - (w_0/c_0). \tag{29}$$

Equation (28) can be simplified as

$$(w/c)K|_{w/c=w_0/c_0} + (w/c)aK_1 \approx C_K \tag{30}$$

here C_K is

$$C_K = (w/c)\left(\frac{\partial \dot{\gamma}^n}{\partial y}\right)^{-1} \frac{\rho}{\rho_s} \frac{\partial u}{\partial t} + \left(\frac{\partial \dot{\gamma}^n}{\partial y}\right)^{-1} \frac{\rho}{\rho_s} \frac{\partial u_s}{\partial t}. \tag{31}$$

In the tiny neighborhood of the w_0/c_0, the following approximation is given

$$\begin{cases} (w/c)K|_{w/c=w_0/c_0} \approx (w_0/c_0)K \\ (w/c)\left(\frac{\partial \dot{\gamma}^n}{\partial y}\right)^{-1} \frac{\rho}{\rho_s} \frac{\partial u}{\partial t} \approx (w_0/c_0)\left(\frac{\partial \dot{\gamma}^n}{\partial y}\right)^{-1} \frac{\rho}{\rho_s} \frac{\partial u}{\partial t} \end{cases}. \tag{32}$$

The values of $\frac{\partial \dot{\gamma}^n}{\partial y}$ and $\frac{\partial u}{\partial t}$ are the constants when the shear rate keeps constant. Substituting Eq. (32) into Eq. (30), we have.

$$(w_0/c_0)K + (w/c)aK_1 \approx C_K. \tag{33}$$

By dividing both sides of Eq. (33) by w_0/c_0, Eq. (34) is obtained as

$$K \approx \frac{C_K}{w_0/c_0} + (w/c)\frac{a_1}{w_0/c_0} \frac{\partial K}{\partial (w/c)} \tag{34}$$

where

$$a_1 = -a. \tag{35}$$

Solving the ordinary Eq. (34), we have

$$K \approx CC_{\mathrm{I}}(w/c)^{CC_{\mathrm{II}}} + b \tag{36}$$

in which CC_{I} is the calculation parameter, CC_{II} and b are

$$CC_{\mathrm{II}} = \frac{w_0/c_0}{w_0/c_0 - w/c} \quad b = \frac{C_K}{w_0/c_0}, \tag{37}$$

In the whole domain, the solution (36) is considered as the basic function. The Bernstein polynomial approximation[29] can be concisely constructed as

$$K \approx D_1(w/c)^{D_2} + D_3 \tag{38}$$

where D_1, D_2 and D_3 are the calculation parameters, and the detailed derivation of Eq. (38) is shown in Appendix I (see the Supplementary Information Appendix I for details). Substituting Eq. (38) into Eq. (19), it is derived

$$\frac{1}{\phi\rho_s} \frac{\partial[\phi\rho_s((w/c)u + u_s)]}{\partial t} \approx \frac{w/c}{\rho} \frac{\partial}{\partial y}\left(\left(D_1(w/c)^{D_2} + D_3\right)\dot{\gamma}^n\right). \tag{39}$$

Expanding Eq. (39), we have

$$\frac{1}{\phi\rho_s}\frac{\partial[\phi\rho_s((w/c)u+u_s)]}{\partial t} \approx \frac{(w/c)\left(D_1(w/c)^{D_2}+D_3\right)}{\rho} n\dot{\gamma}^{n-1}\frac{\partial\dot{\gamma}}{\partial y}. \tag{40}$$

Then, n can be expressed as

$$n \approx \frac{\rho}{(w/c)\left[D_1(w/c)^{D_2}+D_3\right]}\left[\frac{1}{\phi\rho_s}\frac{\partial[\phi\rho_s((w/c)u+u_s)]}{\partial t}\right]\left(\dot{\gamma}^{n-1}\frac{\partial\dot{\gamma}}{\partial y}\right)^{-1} \tag{41}$$

which is the implicit solution of n. The solution is complicated and therefore hard for engineering applications. For simplification, the n is expanded in the neighborhood of $w/c = w_0/c_0$ as

$$n \approx f_0 + f_1(w/c - w_0/c_0) + f_2(w/c - w_0/c_0)^2 + \cdots \tag{42}$$

and the first-order approximation is

$$n \approx f_0 + f_1(w/c - w_0/c_0) \tag{43}$$

in which f_0 is

$$f_0 = n|_{w/c=w_0/c_0} \tag{44}$$

and f_1 is

$$f_1 = \frac{\partial n}{\partial(w/c)}|_{w/c=w_0/c_0}. \tag{45}$$

It is taken the parameters as

$$C_1 = f_1, \quad C_2 = f_0 - (w_0/c_0)f_1. \tag{46}$$

When the value of f_0 is

$$f_0 = (w_0/c_0)f_1 \tag{47}$$

which means the parameter $C_2 = 0$, and n is

$$n \approx C_1 w_0/c_0. \tag{48}$$

Due to the arbitrariness of w_0/c_0, the general form of n is presented as.

$$n \approx C_1 w/c. \tag{49}$$

Substituting Eq. (38) and Eq. (49) into Eq. (16), the four-parameter constitutive model is given as.

$$\eta = \left[D_1(w/c)^{D_2}+D_3\right]\dot{\gamma}^{C_1 w/c-1}. \tag{50}$$

Equation (50) describes the functional relation between the shear stress and the shear rate of cement pastes with varying w/c. It should be noticed that the w/c can be replaced with w/b based on the assumption in Eq. (14).

The apparent viscosity model with SP

This section discusses the apparent viscosity model with the SP which has the chemical structure as shown in Fig. 2. Its specific density is 1.07 g/cm^3, with the side chain length (average number of ethylene oxide units) of 53. The average molecular weight is 58.2×10^3 g/mol, and the polydispersity index is 2.0[18].

The SP mainly disperses cement particles through electrostatic repulsion and steric hindrance after adsorption[30,31]. The electrostatic repulsion force F_e is

$$F_e = k\frac{q_1 q_2}{r^2} \tag{51}$$

where k is the Coulomb's constant, q_1 and q_2 are the charges of ions, r is the distance between two ions. When the type of SP is given, the k, q_1 and q_2 are known. The distance r is related to the number or the concentration of ions in a certain space, which means the whole electrostatic repulsion force F_{et} is

$$F_{et} = \int_\Omega k\frac{q_1 q_2}{r(n_S)^2}\mathrm{d}V \tag{52}$$

in which n_S is the dosage of the SP in a fluid domain Ω. The steric hindrance describes how the physical structure of SP affects its ability to react. Its force F_s can be approximated as a constant for the SP. Introducing F_{et} and F_s into Eq. (4), it is obtained

$$\frac{\partial(\phi^c\rho u)}{\partial t} = \phi^c\frac{\partial}{\partial y}\left(\eta\frac{\partial u}{\partial y}\right) + \phi^c\rho f_x + F_n. \tag{53}$$

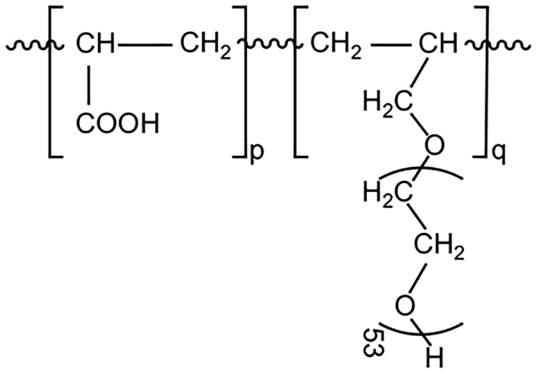

Figure 2. The chemical structure of the main component of the SP[18].

where F_n is.

$$F_n = F_{et} + \phi^c F_s. \tag{54}$$

According to Eq. (52), F_{et} is related to the dosage of the SP, which means F_n in Eq. (54) is the function of n_S. Substituting Eqs. (6)–(7) into Eq. (53), we have

$$\frac{\partial[(1-\phi)\rho u + \phi\rho_s u_s]}{\partial t} - F_n = (1-\phi)\frac{\partial}{\partial y}\left(\eta\frac{\partial u}{\partial y}\right) \tag{55}$$

In a tiny domain $(y, y+\Delta y)$, Eq. (55) can be approximated as

$$\frac{1}{\phi\rho_s}\frac{\partial[\phi\rho_s((w/b)u+u_s)]}{\partial t} + \frac{1}{\phi\rho_s}F_n \approx \frac{w/b}{\rho}\frac{\partial}{\partial y}\left(\frac{\partial u}{\partial y}\right)\eta \tag{56}$$

which can be changed into

$$\eta \approx \left[\frac{w/b}{\rho}\frac{\partial}{\partial y}\left(\frac{\partial u}{\partial y}\right)\right]^{-1}\left[\frac{1}{\phi\rho_s}\frac{\partial[\phi\rho_s((w/b)u+u_s)]}{\partial t} + \frac{1}{\phi\rho_s}F_n\right]. \tag{57}$$

When the influence of the SP is ignored, F_n equals zero. The apparent viscosity η in Eq. (57) is reduced to Eq. (13), which can be approximated as the four-parameter model from Eq. (50).

$$\eta = \left[D_1(w/c)^{D_2} + D_3\right]\dot{\gamma}^{C_1 w/c-1}. \tag{58}$$

Based on Eq. (57), it is considered that the influence of SP comes from the additional item $\left[\frac{w/b}{\rho}\frac{\partial}{\partial y}\left(\frac{\partial u}{\partial y}\right)\right]^{-1}\frac{1}{\phi\rho_s}F_n$, which also can affect the other parameters in Eq. (58). A modified item is added to illustrate the effect of SP in Eq. (58) and the expression of the apparent viscosity is constructed as

$$\eta = \left[D_1(w/c)^{D_2} + D_3\right]\dot{\gamma}^{C_1 w/c-1} + f_3(w/b, n_S). \tag{59}$$

where $f_3(w/b, n_S)$ is the additional modified item, in $(y, y+\Delta y)$, f_3 is

$$f_3(w/b, n_S) = \left[\frac{w/b}{\rho}\frac{\partial}{\partial y}\left(\frac{\partial u}{\partial y}\right)\right]^{-1}\frac{1}{\phi\rho_s}F_n. \tag{60}$$

According to the Bernstein first-order approximation (see the Appendix I for details), considering the effect of SP to D_1 and C_1, the viscosity of whole domain in an arbitrarily known y position is approximated as

$$\eta \approx F_1(n_S)\left[d_1(w/b)^{D_2} + d_3\right]\dot{\gamma}^{F_2(w/b,n_S)w/b-1} + F_3(w/b, n_S) \tag{61}$$

in which d_1 and d_3 are the calculation parameters. $F_1(n_S)$ is the effective coefficient of the dosage of the SP, and $F_3(w/b, n_S)$ owns the same dimension of $\left[\frac{w/b}{\rho}\frac{\partial}{\partial y}\left(\frac{\partial u}{\partial y}\right)\right]^{-1}\frac{1}{\phi\rho_s}F_n$. The detailed expressions of F_1, F_2 and F_3 are shown in Appendix II (see the Supplementary Information Appendix II for details).

The verification of the developed models with varying w/c (or w/b) and SP

In this section, the developed models are verified by being compared with the examples of the experimental results in rheological tests with different w/c and SP of cement pastes.

Different *w/c* (or *w/b*) for cement pastes

Three examples are given from the experimental results of Rosquoët et al.[22], Cyr et al.[26], and Jeong et al.[4] to verify the developed model with *w/c*.

In the experiment of Rosquoët et al.[22], the Portland cement CEM I 52.5 PM ES CP2 is used. The Bogue compositions of the cement are listed as follows: C_3S 63.30%, C_2S 17.90%, C_3A 4.74%, and C_4AF 5.62%[22].All measurements used a Rheomat 115 rheometer with an MS 145 coaxial cylinder spindle. A thermal control system maintains a constant temperature in the test. Tests were conducted at 0.5 min after mixing and at a temperature of 20 ± 1 °C. For each *w/c*, the measurements are conducted by increasing the shear rate from 23 s^{-1} to 1200 s^{-1}. For each shear rate, the shear stress was measured after a minimum of 30 s without fluctuation[22]. Four experimental testing points with *w/c* = 0.5 were chosen as the collocation points to solve the calculation parameters in Eq. (50) as

$$D_1\text{=-0.791497}, D_2 = 1.001, D_3 = 1.36931, C_1 = -0.88272. \tag{62}$$

Compared with the other results in the experiment, the results of the developed model are shown in Figs. 3 and 4 In the two figures, the values of the apparent viscosity plunge before the shear rate reaches 100 s^{-1}. Then, the descending rates slow when the shear rate further increases from 200 s^{-1} to 1000 s^{-1}. The maximum viscosity is about 0.325 Pa·*s* for *w/c* = 0.4. The calculated results agree with the measured[22].

The second verification is conducted based on the measured results from Cyr et al.[26]. The Bogue compositions of the cement used are listed as follows: C_3S 60%, C_2S 13%, C_3A 10%, C_4AF 6%, Gypsum 5%, and others 6%[26]. The apparatus used was a modified Rotovisco RV2 (Haake) with a six-blade vane. The pastes were mixed for 8.5 min to obtain a good dispersion of the components[26]. When the influence of gypsum and other ingredients is ignored, the value of *w/c* equals that of *w/b*. There are four experimental points of the curve with *w/b* = 0.3 used to solve the parameters in Eq. (50) as

$$D_1 = 0.154807, \quad D_2 = -5.3451966, \quad D_3 = -0.989956, \quad C_1 = 1.174112. \tag{63}$$

The calculated results of the developed model and the measured results are shown in Fig. 5. The curve with *w/b* = 0.3 shows that the shear stress increases from 0 to 379 Pa with the shear rate increasing. The calculated results match the measured results[26].

The third verification is based on the test results from the experiment of Jeong et al.[4]. The chemical compositions of the cement used are listed as follows: CaO 60.84%, SiO_2 13.26%, Na_2O 10.05%, SO_3 3.59%, Al_2O_3 3.42%, Fe_2O_3 3.14%, MgO 2.35%, K_2O 1.17%, and others 2.18% (all by the weight percentage of the cement)[4]. The matrix was mixed at low speed for 1 min, halting for 1.5 min, and then was mixed for another 0.5 min at high speed. The matrix was placed in the rheometer right after the mixing. The protocol of the rheological test consists of pre-shearing for 0.5 min at a shear rate of 500 s^{-1}. The pre-shearing procedure avoids memory effects, e.g., the thixotropic effect[4]. Four experimental results of the shear stress-shear rate curve with *w/c* = 0.6 are chosen as the collocation points to solve the calculation parameters in Eq. (50) as

$$D_1 = 0.344347, \quad D_2 = -6.112651, \quad D_3 = 0.75678866, \quad C_1 = 0.77509. \tag{64}$$

Compared with the other measured results in the experiment of Jeong et al.[4], the calculated results of the developed model are presented in Figs. 6 and 7.

The shear stress increases as the shear rate increases, which is applicable for pastes with *w/c* from 0.3 to 0.6, as shown in Figs. 6 and 7. The maximum shear stress is around 2600 Pa, measured in the paste with *w/c* = 0.3 at the shear rate of 1000 s^{-1}. The difference can be observed between the calculated results of the developed model and the measured results at low shear rates, especially for the paste with *w/c* = 0.3. Two reasons result in the difference. First, the test results of cement paste with w/c = 0.6 were used to calibrate the four parameters of the model. Based on these parameters, the rheological behaviours of the other pastes were predicted and compared with the experimental results. For the cement paste with w/c = 0.3, its rheological behaviour is different from the paste with w/c = 0.6. When the w/c = 0.3, the paste behaves like a solid-like system before the shear stress reaches the static yield stress of the paste. After the shear stress exceeds the static yield stress, the paste starts to flow. For the paste with w/c = 0.6, the paste is nearly liquid-like and it starts flowing without a clear-cut yield stress[4]. The parameters are calibrated from the paste with w/c = 0.6 and lead to the variation for the paste with w/c = 0.3 at the low shear rate. As the shear rate increases, the flow resistance from the yield stress of the paste accounts for diminishingly and the variation reduces.

The second reason lies in the measurement protocol in Jeong's research. In the measurement, fresh samples were left standing for 0.5 min after the preshear procedure. The 0.5 min is regarded as the minimum time interval to wait between the preshear and the successive measurement[4]. Then, the rotational speed of the rheometer starts to increase from zero. The paste changed from a flow state in the pre-shearing to a static state at the end of the standing time. The standing time enables the paste with w/c = 0.3 to recover to a solid-like system with static yield stress. Based on the abovementioned two points, the variation between test results and the proposed models can be observed for the paste with w/c = 0.3.

Different *w/b* and SP for cement pastes

The test results from the experiment of Liu et al.[18] in Fig. 1 were used for another verification. The chemical compositions of the cement used are listed as follows: CaO 63.80%, SiO_2 19.41%, Al_2O_3 4.33%, SO_3 3.89%, Fe_2O_3 2.91%, MgO 1.29%, Na_2O 1.29%, K_2O 0.68%, and TiO_2 0.28% (all by the weight percentage of the cement)[18].

Four groups of mixed proportions are chosen with different *w/b* and SP, which are presented in Table 1.

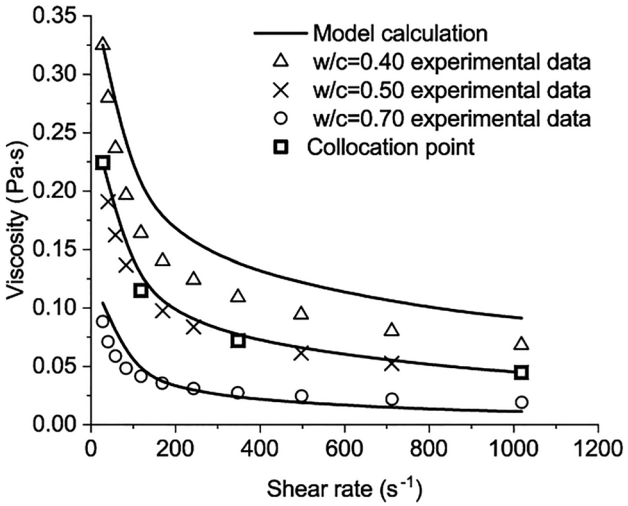

Figure 3. The comparison between model calculation and the experimental data when w/c = 0.4, 0.5, 0.7.

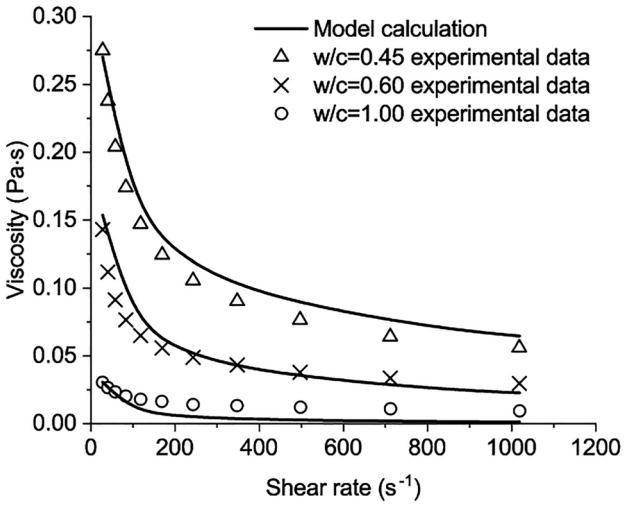

Figure 4. The comparison between model calculation and the experimental data when w/c = 0.45, 0.60, 1.00.

The apparent viscosity, defined as the ratio of shear stress to the shear rate, was measured using a Brookfield R/S SST2000 rheometer with Spindle CC25. Since the shear rate during concrete pouring was from 10 s^{-1} to 20 s^{-1}, the maximum shear rate for the pastes was set to 25 s^{-1}[118]. After placing the paste into the rheometer, the sample was left to equilibrate for 0.5 min and then sheared at a constant rate of 25 s^{-1} for 1 min. The collocation points are chosen from the curve with SP = 2 and $w/b = 0.16$, and the calculation parameters are solved as

$$\begin{aligned} &d_1 = -17.78758, \quad D_2 = 0.78808, \quad d_3 = 7.396649, \quad \lambda = -4.301, \quad \alpha_1 = 1.17071, \\ &\alpha_2 = -11.72098, \quad \alpha_3 = 136.3292, \quad \beta_1 = 0.11854, \quad \beta_2 = -2.98819, \quad \beta_3 = 17.8869 \end{aligned} \tag{65}$$

Compared with the measured results, the calculated results of the present model are shown in Fig. 8. Figure 8 shows the changes in the viscosity of cement pastes with different w/b and SP. When $w/b = 0.32$, the viscosity monotonically decreases with SP = 0.5% (the minimum SP dosage). The other curves in Fig. 8a change from flat to monotonically increasing as the increase of the shear rate. The same phenomena are observed in Fig. 8b and c. In Fig. 8d, all curves monotonically increase as the shear rate increases. The maximum value of the viscosity is 8.448 Pa·s with $w/b = 0.16$, SP = 2.2%, and a shear rate of 25 s^{-1}. The results of the developed model have the same trend of viscosity and agree with the experimental data.

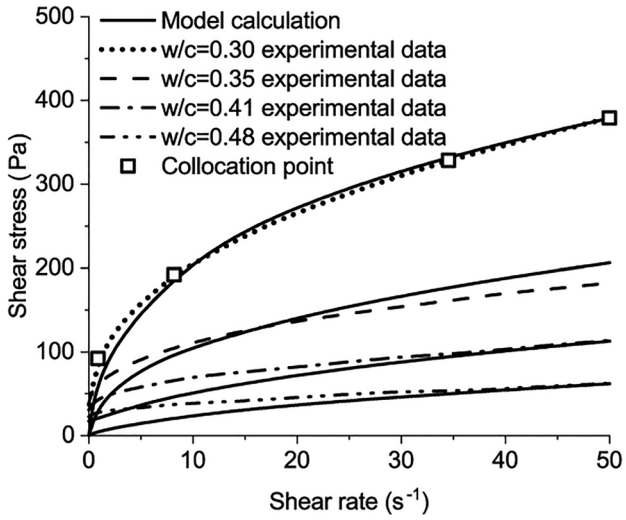

Figure 5. The comparison between model calculation and the experimental data when w/b = 0.30, .035, 0.41, 0.48.

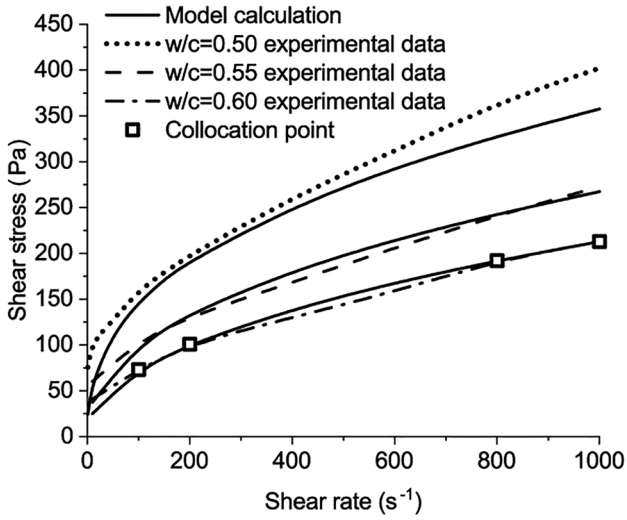

Figure 6. The comparison between model calculation and the experimental data when w/c = 0.50, 0.55, 0.60.

The models can be used to calculate the viscosity of cement pastes and give technique support for the pumping process of cement pastes, e.g., long-distance pumping[32], oil-well cementing[14], and cementitious pastes grouting[33]. In these applications, the viscosity of the cementitious materials is important. With the models proposed in the paper, the effect of adjusting the water-cement ratio and adding superplasticizer on the viscosity of the pastes can be quantified and serves these applications.

Conclusions

The paper presents a mathematical model for the apparent viscosity of cement pastes with varying water-cement/binder ratios and the influence of polycarboxylate-based superplasticizers (SP). The following conclusions can be drawn:

(1) An ordinary differential equation is developed considering the *w/b* and parameter K in the Ostwald model. It is derived based on the Navier–Stokes equations and the Ostwald model of shear stress-shear rate relations;

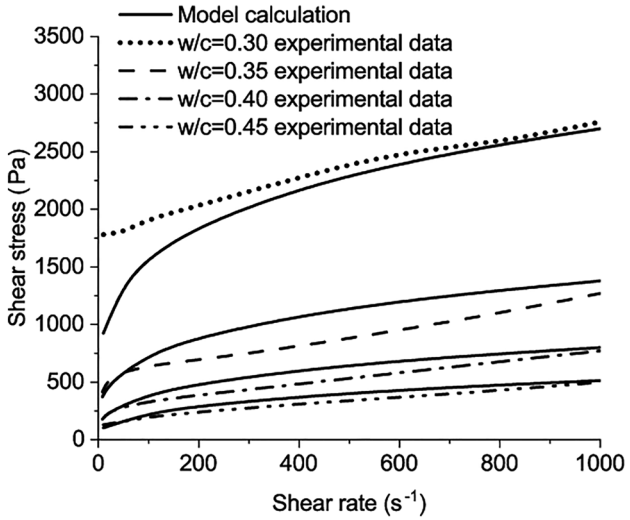

Figure 7. The comparison between model calculation and the experimental data when w/c = 0.3, 0.35, 0.40, 0.45.

Groups	Water-binder ratio	SP Dosage (%)	Cement (%)	Silica fume (%)	Ultra-fine slag (%)
Group 1	0.32	0.5, 0.6, 0.7, 0.8	75	10	15
Group 2	0.24	0.8, 1.0, 1.2, 1.4			
Group 3	0.20	1.3, 1.5, 1.7, 1.9			
Group 4	0.16	1.6, 1.8, 2.0, 2.2			

Table 1. Mix proportions[18].

(2) The whole domain constitutive relation of a four-parameter formula of cement pastes in the rheological stage is approximated by the first-order Bernstein polynomial approximation with different water-cement/binder ratios;

(3) An approximate expression of the viscosity for one type of polycarboxylate-based superplasticizer is constructed considering the result of electrostatic repulsion and steric hindrance;

(4) The developed models are verified by several rheological experiments with different water-cement/binder ratios and dosages of superplasticizers.

It should be noted that the developed models are applicable during the initial mixing stage of cement pastes. Further studies are needed to consider the influence of other factors such as the degree of hydration and the addition of aggregates and other additives on the rheological behaviour of cement-based mixtures.

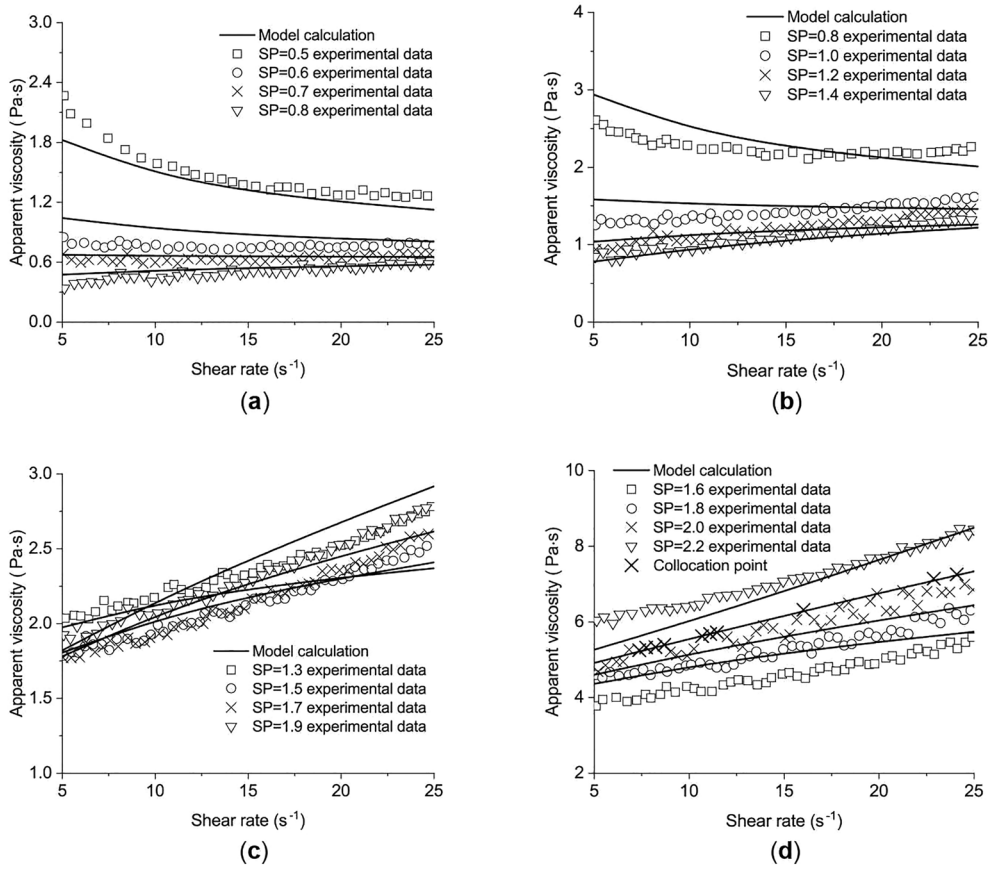

Figure 8. The comparison between model calculation and the experimental data for different w/b and SP. (**a**) paste with w/b = 0.32, (**b**) paste with w/b = 0.24, (**c**) paste with w/b = 0.20, (**d**) paste with w/b = 0.16.

Data availability

The datasets used and/or analysed during the current study are available from the corresponding author upon reasonable request.

Received: 20 April 2023; Accepted: 29 November 2023
Published online: 15 December 2023

References

1. Chidiac, S. & Mahmoodzadeh, F. Plastic viscosity of fresh concrete–A critical review of predictions methods. *Cem. Concr. Compos.* **31**, 535–544 (2009).
2. Marar, K. & Eren, Ö. Effect of cement content and water–cement ratio on fresh concrete properties without admixtures. *Int. J. Phys. Sci.* **6**(24), 5752–5765 (2011).
3. Gupta, M. The effect of water to cement ratio on early age properties of cement paste and mortar by UPV. *Int. J. Eng. Sci.* **5**, 550–556 (2016).
4. Jeong, J., Chuta, E., Ramézani, H. & Guillot, S. Rheological properties for fresh cement paste from colloidal suspension to the three-element Kelvin–Voigt model. *Rheol. Acta* **59**, 47–61 (2020).
5. Aïtcin, P. C. in *Science and Technology of Concrete Admixtures* Ch. The importance of the water–cement and water–binder ratios, 3–13 (Woodhead Publishing, 2016).
6. Einstein, A. *Eine neue bestimmung der moleküldimensionen*, ETH Zurich, (1905).
7. Justnes, H. & Vikan, H. Viscosity of cement slurries as a function of solids content. *Annu. Trans. Nord. Rheol. Soc.* **13**, 75–82 (2005).
8. Struble, L. & Sun, G. K. Viscosity of Portland cement paste as a function of concentration. *Adv. Cem. Based Mater.* **2**, 62–69 (1995).
9. Hodne, H., Galta, S. & Saasen, A. Rheological modelling of cementitious materials using the Quemada model. *Cem. Concr. Res.* **37**, 543–550 (2007).
10. Skare, E. L. *et al.* Rheology modelling of cement paste with manufactured sand and silica fume: Comparing suspension models with artificial neural network predictions. *Constr. Build. Mater.* **317**, 126114 (2022).
11. Bingham, E. C. *Fluidity and Plasticity*. Vol. 2 (McGraw-Hill, 1922).
12. Li, M., Han, J., Zhou, Y. & Yan, P. A rheological model for evaluating the behavior of shear thickening of highly flowable mortar. *Molecules* **26**, 1011 (2021).
13. Peng, J., Deng, D., Liu, Z., Yuan, Q. & Ye, T. Rheological models for fresh cement asphalt paste. *Constr. Build. Mater.* **71**, 254–262 (2014).
14. Tao, C., Kutchko, B. G., Rosenbaum, E. & Massoudi, M. A review of rheological modeling of cement slurry in oil well applications. *Energies* **13**, 570 (2020).

15. Campos, R. & Maciel, G. Test protocol and rheological model influence on determining the rheological properties of cement pastes. *J. Build. Eng.* **44**, 103206 (2021).
16. Rubio-Hernández, F. J. Rheological behavior of fresh cement pastes. *Fluids* **3**, 106 (2018).
17. Vipulanandan, C. & Mohammed, A. Smart cement rheological and piezoresistive behavior for oil well applications. *J. Pet. Sci. Eng.* **135**, 50–58 (2015).
18. Liu, J. *et al.* Influence of superplasticizer dosage on the viscosity of cement paste with low water-binder ratio. *Constr. Build. Mater.* **149**, 359–366 (2017).
19. Jones, T. & Taylor, S. A mathematical model relating the flow curve of a cement paste to its water/cement ratio. *Mag. Concr. Res.* **29**, 207–212 (1977).
20. Lapasin, R., Longo, V. & Rajgelj, S. Thixotropic behaviour of cement pastes. *Cem. Concr. Res.* **9**, 309–318 (1979).
21. Ivanov, Y. & Roshavelov, T. in *Rheology of Fresh Cement and Concrete: Proceedings of an International Conference, Liverpool* (ed Banfill P. G. F) 23–26 (Taylor & Francis).
22. Rosquoët, F., Alexis, A., Khelidj, A. & Phelipot, A. Experimental study of cement grout: Rheological behavior and sedimentation. *Cem. Concr. Res.* **33**, 713–722 (2003).
23. Flatt, R. J. & Bowen, P. Yodel: A yield stress model for suspensions. *J. Am. Ceram. Soc.* **89**, 1244–1256 (2006).
24. Ukrainczyk, N., Thiedeitz, M., Kränkel, T., Koenders, E. & Gehlen, C. Modeling SAOS yield stress of cement suspensions: Microstructure-based computational approach. *Materials* **13**, 2769 (2020).
25. Ma, S. & Kawashima, S. A rheological approach to study the early-age hydration of oil well cement: Effect of temperature, pressure and nanoclay. *Constr. Build. Mater.* **215**, 119–127 (2019).
26. Cyr, M., Legrand, C. & Mouret, M. Study of the shear thickening effect of superplasticizers on the rheological behaviour of cement pastes containing or not mineral additives. *Cem. Concr. Res.* **30**, 1477–1483 (2000).
27. Kundu, P. K., Cohen, I. M. & Dowling, D. R. *Fluid Mechanics* 6th edn, Vol. 1 (Academic Press, 2015).
28. Derksen, J. Simulations of dense agitated solid–liquid suspensions—Effects of the distribution of particle sizes. *Chem. Eng. Sci.* **189**, 56–64 (2018).
29. Farouki, R. T. The Bernstein polynomial basis: A centennial retrospective. *Comput. Aided Geom. Des.* **29**, 379–419 (2012).
30. Faraday, M. V. Experimental researches in electricity. *Philos. Trans. R. Soc. Lond.* **122**, 125–162 (1832).
31. Yoshioka, K., Sakai, E., Daimon, M. & Kitahara, A. Role of steric hindrance in the performance of superplasticizers for concrete. *J. Am. Ceram. Soc.* **80**, 2667–2671 (1997).
32. Feys, D., De Schutter, G., Fataei, S., Martys, N. S. & Mechtcherine, V. Pumping of concrete: Understanding a common placement method with lots of challenges. *Cem. Concr. Res.* **154**, 106720 (2022).
33. Anagnostopoulos, C. A. Effect of different superplasticisers on the physical and mechanical properties of cement grouts. *Constr. Build. Mater.* **50**, 162–168 (2014).

Acknowledgements

The authors of this paper are indebted to the financial support from the National Key R&D Programme Intergovernmental Cooperation on International Science and Technology Innovation (No. 2021YFE0114100), the Sino-German Center for Research Promotion (No. GZ 1574), Science and Technology Commission of Shanghai Municipality (No. 21DZ1203505), and Science and Technology Project of Department of Transportation of Jiangxi Province (No. 2021C0008).

Author contributions

Y.Y.: Conceptualization, Methodology, Writing—original draft. X.W.: Methodology, Verification, Writing—review & editing. X.C.: Methodology, Verification, Visualization. P.X.: Writing—review & editing. E.K.: Project administration. Y.D.: Supervision.

Competing interests

The authors declare no competing interests.

Additional information

Supplementary Information The online version contains supplementary material available at https://doi.org/10.1038/s41598-023-48748-4.

Correspondence and requests for materials should be addressed to Y.D.

Reprints and permissions information is available at www.nature.com/reprints.

Publisher's note Springer Nature remains neutral with regard to jurisdictional claims in published maps and institutional affiliations.